Seed Biology

ARTICLE

Open Access

https://doi.org/10.48130/seedbio-0025-0021

Seed Biology **2025**, 4: e022

RsMYB28 activates the glucosinolates biosynthesis in rapeseed (*Brassica napus* L.) Ogu CMS restorer line

Shuxiang Mao[1,2#], Yaqi Deng[1,2,3#], Dawei Zhang[2,3], Siying Zhu[1,2,3], Jiamin Cui[1,2,3], Chunjun He[1,2,3], Lei Qin[1,2], Tonghua Wang[1,2], Bao Li[1,2], Lili Liu[2,3], Mei Li[1,2] and Mingli Yan[1,2*]

[1] *Hunan Engineering Research Center of Hybrid Rapeseed, Crop Research Institute, Hunan Academy of Agricultural Sciences, Changsha 410125, China*
[2] *Yuelushan Laboratory, Changsha 410128, China*
[3] *Hunan Key Laboratory of Economic Crops Genetic Improvement and Integrated Utilization, School of Life and Health Sciences, Hunan University of Science and Technology, Xiangtan 411201, China*
[#] Authors contributed equally: Shuxiang Mao, Yaqi Deng
[*] Corresponding author, E-mail: ymljack@126.com

Abstract

Glucosinolates (GSLs), primarily found in Brassicaceae species, endow plants with functions in enhancing defense, providing therapeutic benefits, and contributing to unique food flavors. In the Ogu CMS restorer lines of rapeseed (*Brassica napus* L.), the introduction of extra radish genome segments contributes to the elevated accumulation of aliphatic glucosinolates (AGSLs) in leaves and seeds. However, the molecular mechanisms underlying AGSL biosynthesis in these restorer lines remain unclear. In this study, the expression profile of genes involved in the glucosinolate (GSL) biosynthesis pathway, were characterized revealing that GSL biosynthesis is most active in the silique pericarps. Through sequence alignment and functional analysis, a foreign RsMYB28 allele was identified and proposed as the key regulator of AGSL biosynthesis in Ogu CMS restorer lines. Functional validation via *RsMYB28* overexpression confirmed its role in promoting AGSL accumulation. RsMYB28 specifically bound to the promoters of *BnaIMDH3* and *BnaCYP83A1*, and activated their transcription. This study elucidates the core function of RsMYB28 in regulating AGSL biosynthesis in Ogu CMS restorer lines, providing a valuable genetic resource for improving rapeseed resistance and quality through breeding.

Citation: Mao S, Deng Y, Zhang D, Zhu S, Cui J, et al. 2025. RsMYB28 activates the glucosinolates biosynthesis in rapeseed (*Brassica napus* L.) Ogu CMS restorer line. *Seed Biology* 4: e022 https://doi.org/10.48130/seedbio-0025-0021

Introduction

Glucosinolates (GSLs) are a class of secondary metabolites unique to plants of the Brassicaceae family[1]. In recent decades, GSLs have attracted great research attention due to the diverse biological properties of their hydrolysis products[2–4]. They are an essential component of the GSL-myrosinase system, the innate defense mechanism in Brassica plants. The production from the GSL-myrosinase system are responsible for the biochemical defense capabilities of Brassicas[1,2]. Therefore, GSLs play an important role in plant biotic stress and abiotic stress[5,6]. In *Arabidopsis thaliana*, GSLs could directly or indirectly regulate stomatal movement to prevent water loss and improve the plant's survival under these drought conditions. The increases in GSLs content could provide higher protection against multiple stresses, such as salinity and heavy metals[5,7]. Also, the GSL-myrosinase system protects plants against herbivores and pathogenic toxins. Additionally, some GSLs and their hydrolysates confer Brassica vegetables with distinct taste and flavor, and the hydrolysates, particularly the well studied sulforaphane, are considered as effective cancer preventive agents[8,9]. The accumulation of GSLs in the vegetative tissues of rapeseed is of significant importance for advancing quality and resistance breeding in this crop.

Glucosinolates were classified according to their precursor amino acids, the aliphatic glucosinolates (AGSLs) derived from methionine, alanine, leucine, isoleucine, valine, or glutamate; indolic glucosinolates (IGSLs) made from tryptophan; aromatic glucosinolates (ArGSLs) synthesize from phenylalanine and tyrosine. AGSLs represent the most diverse group in Brassicas[1]. The AGSLs biosynthesis pathway involves three major phases: side chain elongation, core structure formation, and side chain modification. The side chain elongation for AGSLs biosynthesis includes branched-chain amino acid aminotransferase (BCAT3/4/6), methylthioalkylmalate synthase (MAM1/2/3), isopropylmalate isomerase large subunit (LeuC1), isopropylmalate isomerase small subunit (LeuD1/2), and isopropylmalate dehydrogenase (IMDH1/2/3)[10,11]. The AGSLs' core structure was metabolized by cytochrome P450 family (CYP79F1/2 and CYP83A1), glutathione S-transferase (GSTF11/U20), gamma-glutamyl peptidase (GGP1) and C-S lyase (SUR1), UDP-glucosyltransferase (UGT74C1), sulfotransferase (SOT16/17/18)[12,13]. AGSLs can undergo side-chain modifications, including flavin monooxygenases ($FMO_{GS\text{-}OXs}$), 2-oxoglutarate- dependent dioxygenases (AOP2/3), and 2-oxo acid-dependent dioxygenase (GS-OH)[14,15].

MYB TFs from the R2R3 subfamily are the most specific transcriptional regulators which involved in GSL biosynthesis[16]. The R2R3 MYBs are further divided into subgroups according to sequence similarity that at least partly correspond with functional conservation[17]. The six members of subgroup 12 positively regulate genes responsible for GSL biosynthesis. MYB28, MYB29, and MYB76, which are known as high AGSL 1 (HAG1), HAG3, and HAG2, respectively, are key players in the modulation of AGSLs biosynthesis in Arabidopsis and Brassica[1,16,18]. MYB34, MYB51, and MYB122 are characterized as essential regulators of IGSL biosynthesis, which is interconnected with indolic phytoalexin[15,16]. MYB28 was identified as a quantitative trait loci (QTL) analysis, which was located within a genomic region that determines AGSL levels[19,20]. MYB28, MYB29, and MYB76 were also identified in a screen for their transactivation potential toward AGSL biosynthetic genes. Overexpression of *MYB28*, *MYB29*, and *MYB76* resulted in AGSLs accumulation increased, the expression

of AGSLs biosynthesis genes was induced. Knock-out mutants of *MYB28* showed significantly decreased levels of short- and long-chain AGSLs, and short-chain AGSLs were reduced in *myb29* mutant. Furthermore, the double mutant *myb28myb29* had almost completely abolished production of AGSLs, which suggested that MYB28 and MYB29 are the master regulators, and MYB76 only plays an accessory role[6].

Utilization of heterosis in rapeseed has proven to be the most important approach for increasing economic traits, which has been achieved through a set of male-sterile line (A line), maintainer line (B line), and restorer line (R line)[21]. The Ogu cytoplasm confers complete male sterility to *Brassica napus* cultivars, and the restorer gene of Ogu cytoplasmic male sterility (CMS) was from radish[22]. Along with the introduction of the Rfo gene into *Brassica napus*, extra segments of the radish genome, which contributes to elevated GSL level, were introgressed into *Brassica napus*[22]. The restorer line for Ogu CMS with high leaf and seed-GSLs, and the genetic and molecular mechanisms involved in restorer line background are rarely studied. In this study, the profiles of GSLs (leaves and mature seeds) and transcriptome (leaves, flowers, silique pericarps and young seeds) in an Ogu CMS restorer line R2260 were investigated, and GSLs biosynthesis gene expression profiles were conducted. A foreign gene-*RsMYB28* was identified, and the role regulating AGSL biosynthesis was validated by enhancing the expression of *RsMYB28*, leading to AGSL accumulation in rapeseed. These findings provide important clues for understanding the molecular mechanisms underlying GSL accumulation in Ogu CMS restorer lines, and for leveraging *RsMYB28* to enhance rapeseed quality and resistance breeding.

Materials and methods

Plant materials and growth conditions

Two rapeseed varieties, R2260 and Westar, were used in the present study, which are preserved in the germplasm bank of Hunan Crop Research Institute. The seedlings were cultivated in a 50-well nursery site and then planted in the experimental base when they had grown four true leaves. The planting density was 20 cm between plants and 25 cm between rows. The field management followed standard agricultural practice. The functional leaves and flowers were sampled at the florescence, and young silique were sampled after pollination for 21 d, the silique pericarps and young seeds were divided and saved individually. All samples were immediately frozen in liquid nitrogen and stored at −80 °C for GSLs determination and RNA-seq. *Nicotiana benthamiana* (*N. benthamiana*) and a part of rapeseed were grown in a plant growth chamber at 22–24 °C and 65% humidity under a 16 h/8 h light/dark photoperiod.

Plasmid construction and plant transformation

Total RNA was isolated by using an RNAprep Pure Plant Kit (CHN, Tiangen, China). Total RNA was reverse transcribed into cDNA by HiScript II Q RT SuperMix for qPCR (+ gDNA wiper) or HiScript II 1st Strand cDNA Synthesis Kit (+ gDNA wiper) for PCR (CHN, Vazyme). *Brassica napus* L. gDNA was extracted by Plant gDNA Extract Kit (CHN, Coolaber). The Phanta Flash Super-Fidelity DNA Polymerase (CHN, Vazyme) was used to amplify all the target gene fragments by polymerase chain reaction (PCR), and the SE Seamless Cloning and Assembly Kit (CHN, Zomanbio) was used to construct the vectors. The primers for the target genes amplification were designed with the inclusion of a 15–20 bp sequence of the vector as the homologous arm and a 15–30 bp target gene sequence (Supplementary Table S1).

To perform over expression of *RsMYB28* in Westar, the full coding sequences of *RsMYB28* was cloned, and the pCAMBIA2306 vectors were used to construct the *RsMYB28* over expression (*RsMYB28*-OE) vector. These constructs were then transformed into *Agrobacterium tumefaciens* (*A. tumefaciens*) strain GV3101, and transformed into Westar according to the method in a previous report[23]. All positive transformants were selected on agar plates supplemented with 50 mg/L Kana.

Determination of glucosinolate content

According to a previously described method[24], the rapeseed leaves and seed powder was extracted with 70% methanol at 75 °C twice, and 5 mg/mL sinigrin was used as an internal standard. The extraction was transferred to DEAE Sephadex A-25 anion-exchange resin column for desulfoGSL isolation by anion-exchange chromatography. desulfoGSL release was achieved on the column by the addition of sulfatase solution (0.5 mg/mL). For 16 h incubation at room temperature, the column was washed with 3 mL of deionized water to collect desulfoGSL.

A series UPLC-MS (USA, Waters) instrument was used in conjunction with ESI in positive ion mode. The analytical column model: Waters 1.8 μm C18 (100 mm × 2.1 mm). The mobile phase consisted of water (A), and methanol (B). Chromatography was performed with a 250 μL/min flow rate at 40 °C, and with the following gradient program: 5% B for 1 min, linear gradient from 5% B to 100% B for 8 min, 100% B for 2 min, and equilibration of 5% B for 2 min. DesulfoGSLs were detected by both a diode array detector at 229 nm and a mass spectrometer with electrospray ionization. The source conditions were as follows: capillary, 3.5 kV; cone, 30 V; extractor, 5 V; source temperature, 120 °C; and desolvation temperature, 350 °C. The spray was stabilized by a cone gas flow of 100 L/h, and the desolvation gas flow was adjusted to 750 L/h. Compounds were identified by comparing the MS data (retention time, ions, and confirmation transition). Internal standard (sinigrin, USA, Sigma-Aldrich) was used for the quantitation of desulfoGSL.

RNA sequencing and analysis

The mRNA was purified using poly-T oligo-attached magnetic beads. The IlluminaNovaseq Platform was used to construct and sequence the stranded RNA libraries. The clean data was filter out and then mapped onto the ZS11 genome. The mapped reads were assembled by StringTie (vl.3.3b). The FeatureCounts (vl.5.0-p3) was used to count the read numbers mapped to each gene. The lengths of the genes and read counts were used to calculate the FPKM of each gene. The DESeq2 R package (1.20.0) was used to analyze the differential expression of two groups. The clusterProfiler R package was used to test the statistical enrichment of KEGG pathways.

Quantitative reverse transcription PCR analysis

The AceQ qPCR SYBR Green Master Mix Kit (CHN, Vazyme) was used to analysis the gene expression of target genes. For the RT-qPCR, the specific primers were designed by the National Center for Biotechnology Information (NCBI, Supplementary Table S1).

Phylogenetic tree construction, chromosome distribution, and promoter structure analysis

The *MYB28* sequence of *Arabidopsis thaliana* was obtained from the TAIR database (www.arabidopsis.org)[25]. The genome data of *B. rapa* (chiifu V4), *B. oleracea* (OX-heart), *B. nigra* (Ni100_LR-v2.0), *B. juncea* (Tumida-T84-66-v1.5), and *B. carinata* (Zd-1-v1.0) from the TBGR database (www.tbgr.org.cn)[26], radish genome data (RS06, RS07, RS08, and RS10) was taken with reference to the report by Zhang et al.[27], and the amino acid sequence of MYB28 proteins in those genomes screened using the BLAST tool of TBtools[28]. Using the phylosuite software[29], the alignment and phylogenetic tree

were executed by Mafft and fast-tree through the NJ method, respectively. To locate the Ogu fertility restorer gene and linked genes on the chromosome, those genes in the *Arabidopsis thaliana* genome which used seeds to identify homologous genes in the radish genome. The distribution location information was collected from the radish genomes, and a gene distribution map was drawn using TBtools. The cis-acting elements in the promoter region were predicted by PlantCARE[30], and displayed using TBtools.

Subcellular localization analysis

The ORFs of *RsMYB28* were inserted into pCAMBIA1300-GFP expression vectors, and introduced into *A. tumefaciens* strain GV3101. The bacterial suspensions were injected into tobacco leaves, and then kept in a chamber for 2–3 d. GFP signals were observed with a confocal laser-scanning microscope.

Dual LUC assays

The *RsMYB28*-OE vector as the effector, and the promoter sequences of *BnaIMDH3* and *BnaCYP83A1* were cloned into the pGreenII 0800-LUC vector as the reporters, which were introduced into *A. tumefaciens* strain and expressed in *N. benthamiana* leaves. Fluorescence was observed using an imaging system (FRA, VILBER, NEWTON7.0 Bio plus), and LUC activity was determined with a LUC detection kit (CHN, Vazyme).

Electrophoretic mobility shift assay (EMSA)

Oligonucleotide probes of *BnaIMDH3* and *BnaCYP83A1* promoters were synthesized and labeled with biotin at the 5' end by Sangon Biotech. The probes were incubated with the nuclear extract at room temperature for 30 min. The entire reaction mixture was run on a non-denaturing 0.5 × TBE 6% polyacrylamide gel for 1 h at 60 V at 4 °C, and then transferred onto Biodyne® B nylon membranes (Pall Corporation). Signals were visualized with reagents included in the kit and ChemiDoc XRS (UAS, Bio-Rad Laboratories).

Statistical analysis

All data are shown as the average value of at least three independent replicates. One-way analysis of variance in was carried out in SPSS version 22 (IBM). Significant differences were determined by the Duncan's test at significance levels.

Results

Aliphatic glucosinolates specific accumulation in R2260

Eleven GSLs were detected by UPLC-MS, including six of AGSLs (Glucoraphanin, RAA; Gluconapin, GNA; Progoitrin, PRO; Glucoalyssin, GAL; Glucobrassicanapin, GBN; Gluconapoleiferin, GNF), four of IGSLs (Glucobrassicin, GBC; 4-Methoxyglucobrassicin, 4ME; 4-Hydroxyglucobrassicin, 4OH; Neoglcobrassincin, NEO), and one of ArGSL (Gluconasturtiin, GNT; Fig. 1, Supplementary Table S2).

All six AGSLs content in R2260 is higher than in Westar, both leaves and seeds, except the PRO in seeds. Not only the content of AGSLs but also the profiles are more abundant in R2260, the GNF was only detected in R2260 seeds. The TAGSL content of R2260 are about 5.1 fold (leaves), and 3.6 fold (seeds) than in Westar; for the 4C-AGSL content of R2260 are about 8.9 fold (leaves), and 3.6 fold (seeds) than in Westar; and the 5C-AGSL content of R2260 are about 3.6 fold (leaves), and 11.4 fold (seeds) than in Westar (Fig. 1, Supplementary Table S2).

The content of AGSLs is higher in seeds than in leaves, for the 4C-AGSLs, there are 2.5 times in R2260, and 9.2 times in Westar; more over, the TAGSL content present is 2.2 times in R2260, and 3.1 times in Westar. However, only 1.8 times in R2260 for 5C-GSLs, and its content is lower in seeds than in leaves (Fig. 1, Supplementary Table S2).

AGSL biosynthetic pathway genes were activated in R2260

Transcriptome analyses were performed for leaf (L), flower (F), silique pericarp (Si), and seed (Se) of R2260 and Westar, to investigate the mechanisms underlying differential AGSLs accumulation. The gene exclusively up-regulated in R2260 than Westar were focused; the Kyoto Encyclopedia of Genes and Genomes (KEGG) pathway enrichment analyses showed that these gene was enriched in 'glucosinolate biosynthesis', except in seeds, and the other pathways related to GSL biosynthesis, such as 'sulfur metabolism', 'tryptophan metabolism', and 'glutathione metabolism' (Fig. 2a, b, and Supplementary Fig. S1). To analyse the key activated pathway, Gene Set Enrichment Analysis (GSEA) was applied with differentially expressed genes. Also, the results showed that the 'glucosinolate biosynthesis' pathway showed specific enrichment in R2260 (leaf,

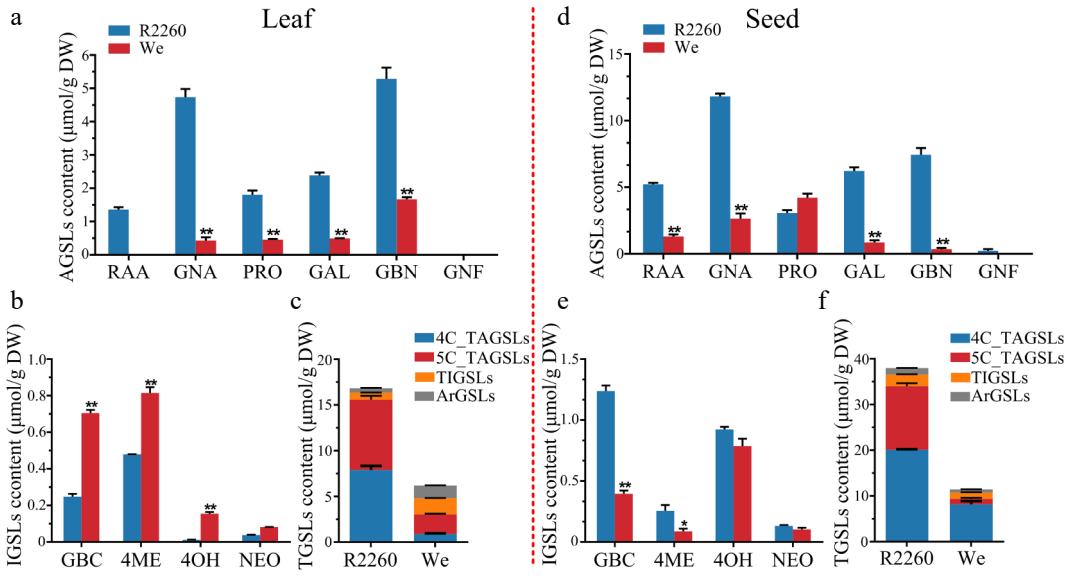

Fig. 1 Content of glucosinolates in R2260 and Westar (We). (a), (d) Aliphatic glucosinolates (AGSLs) content in leaves and seeds; (b), (e) Indolic glucosinolates (IGSLs) content in leaves and seeds; (c), (f) Total glucosinolates (TGSLs) content in leaves and seeds. Each value is the mean of three replicates. The vertical bar indicates the standard error. Asterisks indicate significant differences (** $p < 0.01$, * $p < 0.05$).

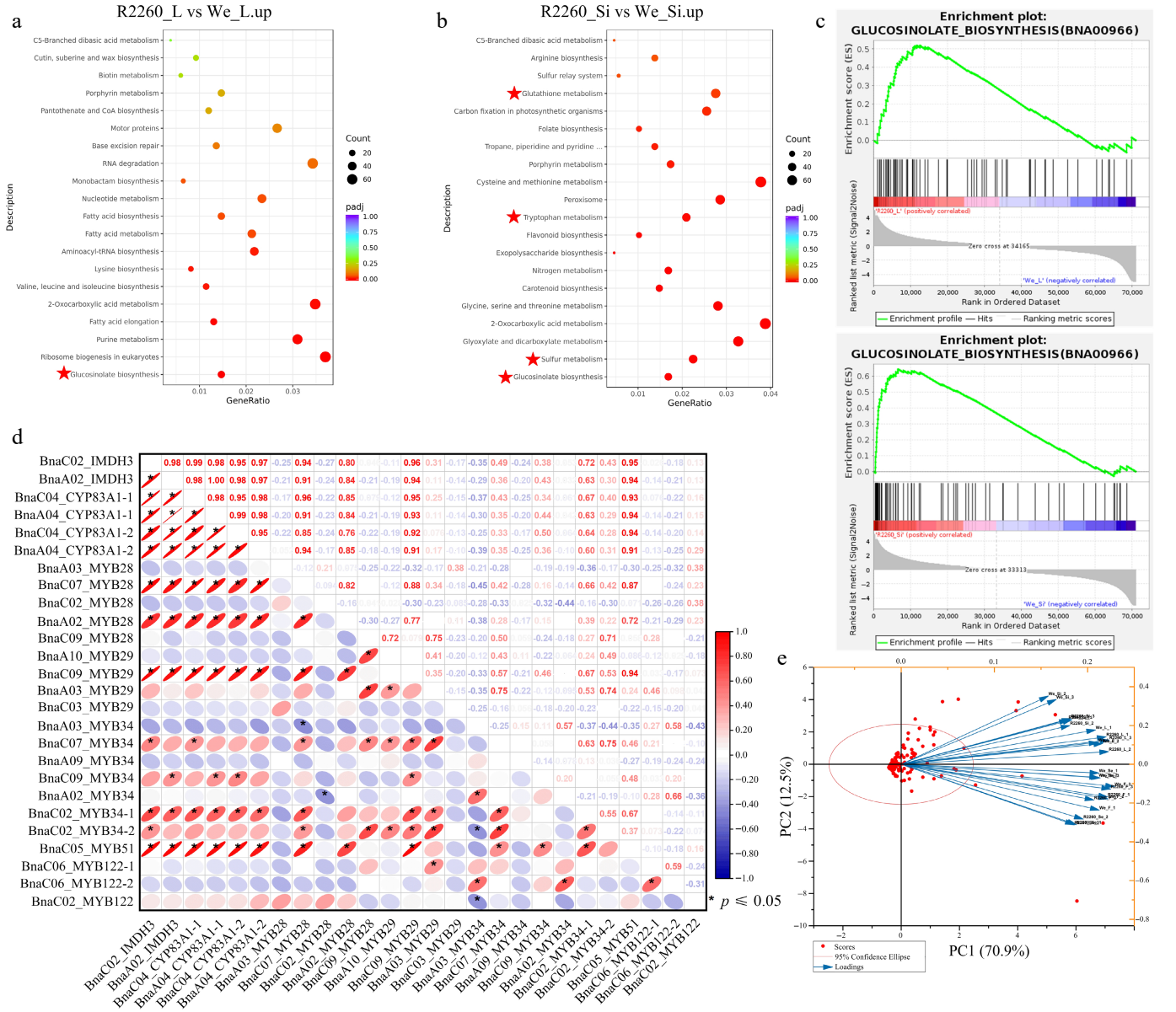

Fig. 2 Transcriptome analysis of R2260 and Westar (We), in leaves (L), flowers (F), silique pericarps (Si), and seeds (Se). (a), (b) KEGG pathway enrichment analysis of differentially expressed genes between R2260-We. (c) Gene Set Enrichment Analysis (GSEA) of differentially expressed genes between R2260-We. (d) Pearson correlation analysis of *BnaIMDH3*, *BnaCYP83A1*, and the MYBs which contribute to glucosinolates biosynthesis. (e) Biplot of the principal component analysis of the observed FPKM values of glucosinolates biosynthesis pathway genes in R2260 and We, with leaves (L), flowers (F), silique pericarps (Si), and seeds (Se).

flower, and silique pericarp) when compared with Westar (Fig. 2c, Supplementary Fig. S2a).

For GSL biosynthesis, a total of 194 core genes and 29 of key transcription factors were identified, which include 34 GSL side chain elongation genes, 74 GSL core structure formation genes, and 86 GSL secondary modification genes (Fig. 3, Supplementary Table S3). The expression level was illustrated by FPKM with heatmaps, in the AGSL side chain elongation stage, among this, genes of *BCAT4* (BnaA03G0359600ZS, BnaC05G0396400ZS, BnaA05G0362200ZS, and BnaC03G0438900ZS), *IIL1* (BnaA08G0054300ZS, BnaC04G0361900ZS, BnaA04G0076900ZS, and BnaC08G0074300ZS), *IPMI2* (BnaC04G0039400ZS and BnaA05G0036500ZS), *IMDH3* (BnaC02G0060000ZS and BnaA02G0052200ZS), and *BCAT3* (BnaA01G0217100ZS and BnaA06G0156700ZS), whose expression value was higher in the R2260 leaf, flower, and silique pericarp than in Westar (Fig. 3, Supplementary Table S3). Meanwhile, the AGSL core structure formation gene expression increased in R2260, which include *CYP79F1* (BnaC05G0136700ZS and BnaA06G0110600ZS), *CYP83A1* (BnaC04G0359300ZS, BnaA04G0267400ZS, BnaC04G0584500ZS, and BnaA04G0074700ZS), *GSTF11* (BnaC05G0546700ZS and BnaA05G0489300ZS), *GSTU20* (BnaC06G0255500ZS and BnaA07G0235200ZS), *SUR1* (BnaC07G0005900ZS and BnaA07G0001300ZS), *UGT74B1* (BnaC05G0210800ZS and BnaA09G0448300ZS), *UGT74C1* (BnaA05G0121200ZS and BnaC04G0153200ZS), *SOT16* (BnaC02G0280500ZS), *SOT17* (BnaA06G0128100ZS), and *SOT18* (BnaC06G0404300ZS; Fig. 3, Supplementary Table S3). The AGSL secondary modification genes presented as the same expression pattern, such as $FMO_{GS\text{-}OX2}$ (BnaA09G0155300ZS and BnaA09G0155200ZS), *AOP2* (BnaC03G0321400ZS, BnaA02G0257300ZS, and BnaC02G0348800ZS), and *GS-OH* (BnaC03G0090500ZS; Fig. 3, Supplementary Table S3).

The Pearson correlation coefficient was used to explore the relationship between GSLs content and the gene expression level in

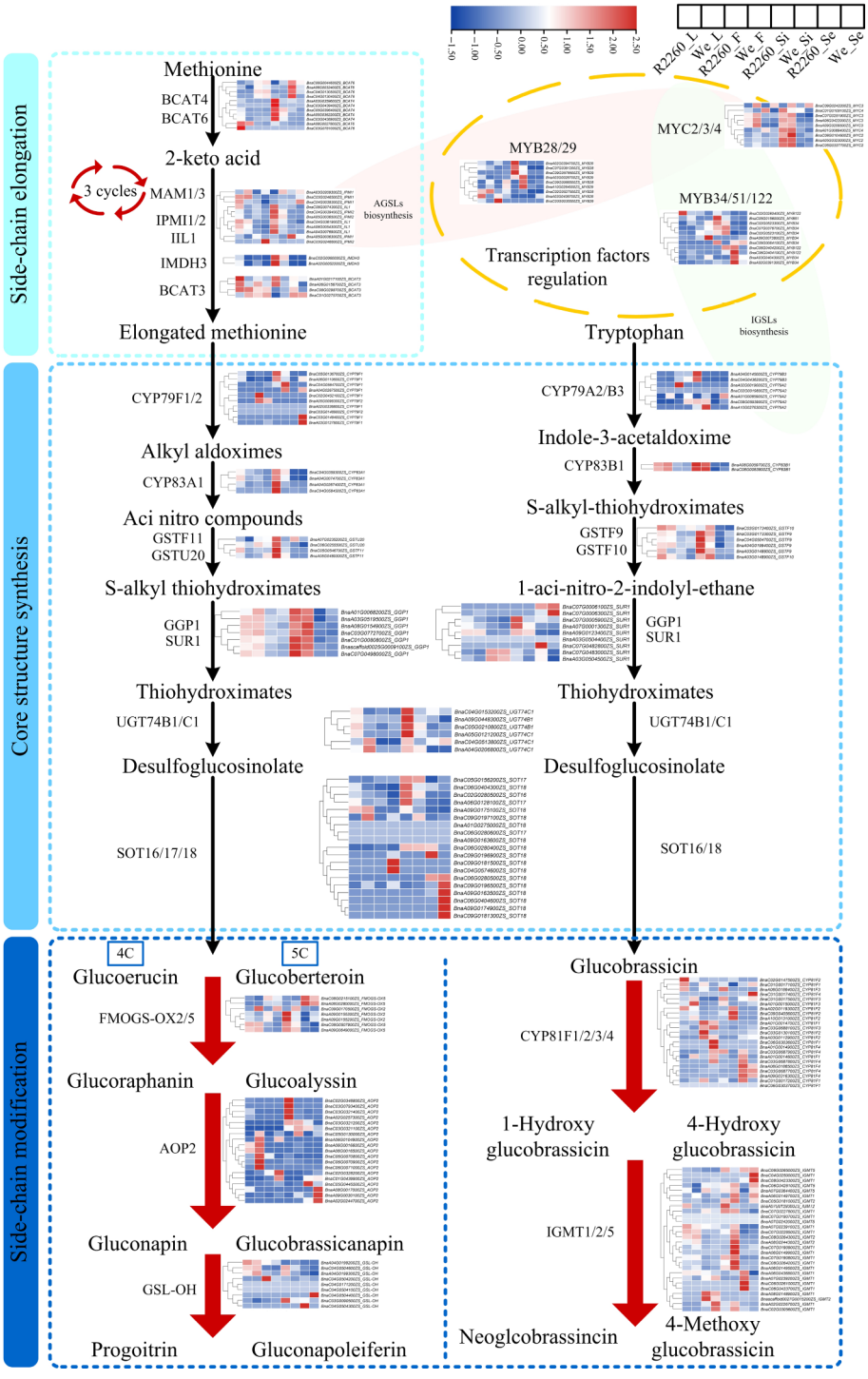

Fig. 3 Expression profile of genes related to glucosinolates biosynthesis in R2260 and Westar (We) of leaves (L), flowers (F), silique pericarps (Si), and seeds (Se), the samples arranged from left to right as R2260_L, We_L, R2260_F, We_F, R2260_Si, We_Si, R2260_Se, We_Se. The FPKM values were used to draw heatmaps, and the red-to-blue gradient in the heatmaps indicates FPKM values from high to low, respectively. Each value is the mean of three replicates.

R2260 and Westar leaves, two important enzymes for AGSL side chain elongation and core structure formation, BnaIMDH3 and BnaCYP83A1 were selected. The analysis showed that the expression pattern of *BnaIMDH3* and *BnaCYP83A1* were significantly positively correlated to AGSL content (Supplementary Fig. S2d), and the key transcription factor (BnaC07G0381200ZS_*MYB28*, BnaA02G03947-00ZS_*MYB28,* and BnaC09G0578500ZS_*MYB29*) expression pattern presented the same correlativity as *BnaIMDH3* and *BnaCYP83A1* (Fig. 2d, Supplementary Table S3). However, the expression of BnaC07G0381200ZS_*MYB28*, BnaA02G0394700ZS_*MYB28,* and BnaC09G0578500ZS_*MYB29* maintain low levels (Fig. 2d, Supplementary Table S3).

Expression level of AGSL biosynthesis genes in R2260 exhibit tissue variability

KEGG pathway enrichment analyses showed that the genes up-regulated in R2260 leaf were enriched in 'glucosinolate

biosynthesis', significantly, when compared with flower and seed (Supplementary Fig. S1). Additionally, the genes of GSL biosynthesis in R2260 and Westar silique pericarp were more active than in leaf (Supplementary Fig. S1). Also, the GSEA indicated that the 'glucosinolate biosynthesis' pathway was activated in R2260 leaf, flower, and silique pericarp, significantly (Supplementary Fig. S2). Principal Component Analysis (PCA) was carried out with GSL biosynthesis gene expression values, which indicate that the GSL biosynthesis capacity of leaves and silique pericarps obtained a positive correlation, flowers, and seeds presented a very strong positive correlation (Fig. 2e). AGSL biosynthesis was more active in leaves and silique pericarps (Fig. 3).

Foreign RsMYB28 is the key transcription factor to promote AGSLs accumulation in R2260

The high accumulation of AGSLs in seeds and leaves is primarily attributed to MYB28, which acts as the predominant regulator of their biosynthesis[31]. Based on the characterization of a radish introgression carrying the Ogu fertility restorer gene and linked genes in rapeseed, these genes were mapped to chromosome 9 of the radish genome. Among these, only *RsMYB28* was localized between the RFO-specific marker (RFO) and a linkage marker (PGI; Supplementary Fig. S3a, Supplementary Table S4). We therefore propose that *RsMYB28* was co-introduced into the rapeseed genome with the RFO segment. Consistent with this, both the RFO-specific marker (RFO) and the linkage marker were detected in R2260 and R2020, but not in Westar (Supplementary Fig. S3b). The sequence of *RsMYB28* was used to design the specific primers following primer design principles (Supplementary Table S1), and the results showed that there is a higher expression level of *RsMYB28* in R2260 when compared with Westar, and *RsMYB28* can not be detected in Westar (Figs. 4b, Supplementary Fig. S4b). Additionally, two *RsMYB28* ORFs were obtained from two restorer lines R2260 and R2020, and they were named as *RsMYB28*_R2260 and *RsMYB28*_R2020 (Supplementary Fig. S4a, Supplementary Table S5).

The amino-acid sequence of MYB28 orthologous in *B. rapa* (chiifu V4), *B. oleracea* (OX-heart), *B. nigra* (Ni100_LR-v2.0), *B. juncea* (Tumida-T84-66-v1.5), *B. carinata* (Zd-1-v1.0), and radish were identified, for the phylogenetic analysis. RsMYB28_R2260 and RsMYB28_R2020 were classified into one group, and RsMYB28_R2260 has a closer phylogenetic relationship with the MYB28 in European radish, however, RsMYB28_R2020 was closer with one MYB28 in all four radishes (Fig. 4a). The amino acid sequence alignment results indicated that RsMYB28_R2260 and RsMYB28_R2020 possessed the MYB family complete conserved domain (Fig. 4d). Only the expression of *BnaC07_MYB28* and *BnaA02_MYB28* in R2260 maintained a positively relationship with AGSL biosynthesis pathway genes (Fig. 2d), and the endogenous MYB28 gene sequences of rapeseed maintain an extremely low degree of variation in R2260, while used the low seed-GSL rapeseed ZS11 as the reference genome (Fig. 4c, Supplementary Fig. S4c and S4d). Further indicating that the foreign RsMYB28 contributes the key role in R2260 AGSL accumulation.

Overexpression of *RsMYB28* induced AGSLs biosynthesis in rapeseed

To investigate the effect of RsMYB28 on AGSL biosynthesis, two *RsMYB28* overexpression (*RsMYB28*_R2260-OE and *RsMYB28*_R2020-OE) vectors were generated and transformed into Westar (Fig. 5a, b and d). Quantitative reverse-transcription polymerase chain reaction (RT-qPCR) was used to assess *RsMYB28* expression in the *RsMYB28*_R2260-OE and *RsMYB28*_R2020-OE lines. A significantly high expression level was detected in three of the *RsMYB28*_R2260-OE lines, and five of the *RsMYB28*_R2020-OE line leaves, and the GSLs content was tested in those transgenic lines (Fig. 5c).

The content of GNA, PRO, and GBN had the greatest improvement in overexpression transgenic lines when compared with WT (Fig. 5e, g and Supplementary Table S6). An approximately 2-fold increase of GNA in *RsMYB28*_R2260-OE-1 and *RsMYB28*_R2020-OE-8 leaves was observed, meanwhile the PRO held about a 2-fold increase in *RsMYB28*_R2260-OE-1/2/6 and *RsMYB28*_R2020-OE-8, GBN content obtained a 4 to 9-fold increase in all transgenic lines. Moreover, GNF accumulated in transgenic lines but was undetected in WT. Gene expression analysis showed that overexpression of *RsMYB28* induced the expression of AGSL biosynthesis-related genes (*BnaIMDH3* and *BnaCYP83A1*; Fig. 6a).

RsMYB28 directly interacts with the promoters of *BnaIMDH3* and *BnaCYP83A1*

The compelling inducible expression of *BnaIMDH3* and *BnaCYP83A1* in *RsMYB28* overexpression lines, inferred that the RsMYB28 protein would directly bind to the promoter of *BnaIMDH3* and *BnaCYP83A1* and regulate their expression (Fig. 6a). The MYB family proteins could bind to the MBS and MRE elements in the promoters. The subcellular localization of RsMYB28 was investigated, and the *RsMYB28* coding sequence was fused with the green fluorescence protein (GFP) sequence and the expression driven by 35S. Green fluorescence was detected in the nucleus, as evidenced by the overlap of the signal with the nucleus subcellular localization marker (Fig. 6b). These results indicate that RsMYB28 could play a transcriptional regulatory function in the nucleus (Fig. 6b).

The promoter sequences of *BnaIMDH3* and *BnaCYP83A1* were analyzed, and the MBS and MRE elements were found in their promoters (Supplementary Fig. S5, Supplementary Table S7). To demonstrate the interaction relationship among RsMYB28, *BnaIMDH3*, and *BnaCYP83A1*, two biotin-labeled probes from *BnaIMDH3* and *BnaCYP83A1* promoter regions, which contain MBS and MRE elements were employed. The EMSA indicated RsMYB28 can directly bind to the specific promoter regions (Fig. 6d). Dual luciferase (LUC) assays were performed to test the transcriptional regulation of RsMYB28 on *BnaIMDH3* and *BnaCYP83A1*. The effector and reporter plasmids were constructed (Fig. 6c), and recombinant plasmids were introduced into Agrobacterium, and expressed in tobacco leaves. The results of fluorescence imaging and LUC activity assays showed that RsMYB28 could directly binding to *BnaIMDH3* and *BnaCYP83A1* promoters and activated their expression (Fig. 6c).

Discussion

To optimize the use of seed meal as animal feed, low seed GSL (< 30 μmol/g) rapeseed cultivars were selected by breeding efforts. However, these cultivars could be more susceptible to pests and diseases due to the reduction of the presumed defensive role of GSL[32]. Plants, being sessile organisms, experience a variety of abiotic and biotic challenges during their life span. They must grow and also defend themselves at the same time to reproduce and optimize their fitness under natural environments[33]. The secondary metabolites of GSLs with unique structural endow the function in plant defense, which enhances the survival rate under abiotic and biotic stresses[34]. Additionally, the hydrolysis production of GSL is well-known to have anti-oxidative and anti-inflammatory properties, which are beneficial to human health[35].

The chemical composition of the variable R-group side chain of the GLSs has a significant effect on the bioactivity of the corresponding hydrolysis production of GSLs. The GSLs composition profiling possessed an essential role for the usefulness of GSLs in rapeseed breeding. Most GSLs in Brassicaceae crops are derived biosynthetically from either methionine (Met), phenylalanine

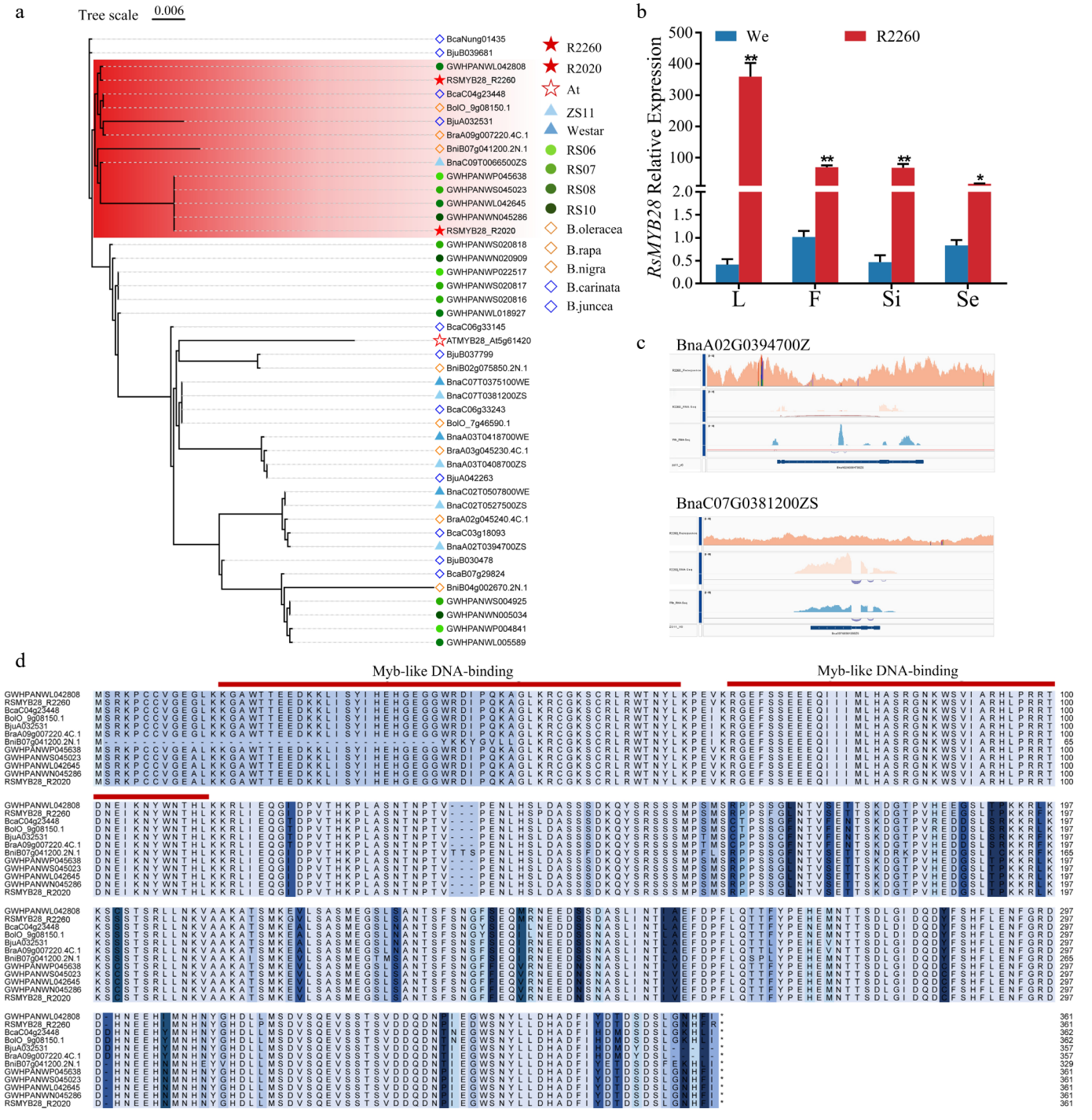

Fig. 4 *RsMYB28* identification and the sequences analysis. (a) Phylogenetic analysis of MYB28s from R2260, R2020, *Arabidopsis thaliana* (At), *Brassica napus* (ZS11 and Westar), *Raphanus sativus* (RS06, RS07, RS08, and RS10), *B. rapa* (chiifu V4), *B. oleracea* (OX-heart), *B. nigra* (Ni100_LR-v2.0), *B. juncea* (Tumida-T84-66-v1.5), and *B. carinata* (Zd-1-v1.0). (b) Relative expression of *RsMYB28* in R2260 and Westar (We) of leaves (L), flowers (F), silique pericarps (Si), and seeds (Se). Each value is the mean of three replicates. The vertical bar indicates the standard error. Asterisks indicate significant differences (** $p < 0.01$, * $p < 0.05$). (c) The gene sequences alignment of *BnaMYB28s* in R2260, We, and ZS11 by IGV. (d) Multiple amino acid sequence alignment of RsMYB28s in *Raphanus sativus* (RS06, RS07, RS08, and RS10), *B. carinata* (Zd-1-v1.0), *B. oleracea* (OX-heart), *B. juncea* (Tumida-T84-66-v1.5), *B. rapa* (chiifu V4), and *B. nigra* (Ni100_LR-v2.0).

(Phe), tyrosine (Tyr), or tryptophan (Trp) . Met-derived AGSLs appear to predominate in most species, both in content and number of structures[8,36–38] (Fig. 1), the TAGSL content in R2260 and Westar accounted the ratio of TGSL with 92.52% (R2260-leaf), 89.57% (R2260-seed), 49.17% (Westar-leaf), and 81.93% (Westar-leaf; Fig. 1f). RAA is the inactive and chemically stable biological precursor of sulforaphane which possess the anticarcinogenic activity, antiviral activity (including COVID-19), anti-inflammatory activity, neuroprotective activity, et al.[39–41], the member of AGSL, obtained the ratio of 8% (R2260-leaf), and 13.76% (R2260-seed) in TGSL (Fig. 1a, d). The accumulation is higher in R2260 than the others previously reported (Fig. 1)[38,42]. What's more, GNA and GBN could provide unique flavors and possess antimicrobial activity, the accumulation was higher in R2260, than Westar. Notably, the PRO, an antinutrient substance, which is recognized as having a goitrogenic effect on livestock-fed protein-rich seed meal, as well as a bitter and spicy

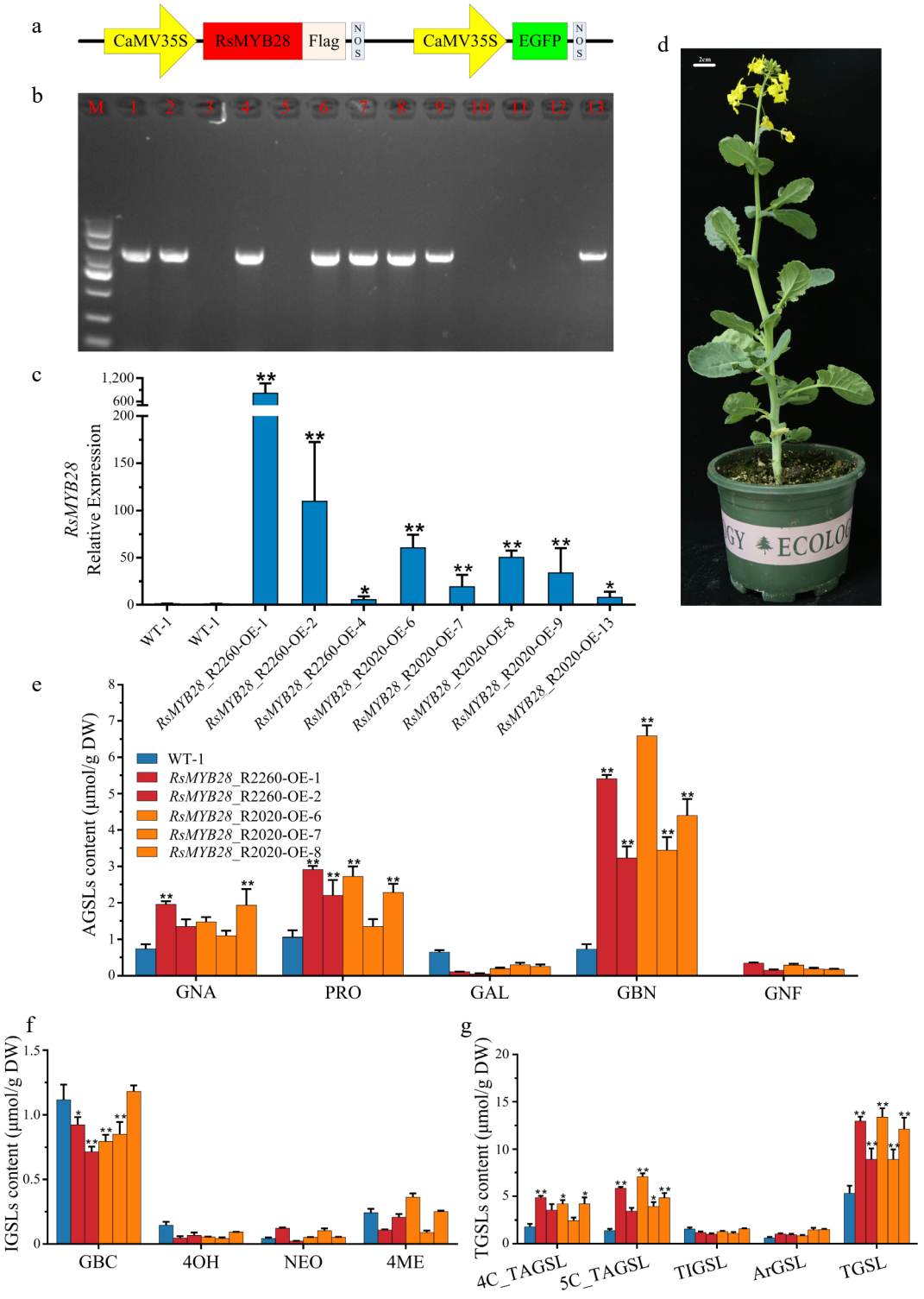

Fig. 5 Biological function identification of RsMYB28. (a) Schematic diagram showing the constructs used for genetic transformation. (b) PCR identification of *RsMYB28*-overexpressing (*RsMYB28*-OE) transgenic lines. (c) Relative expression of *RsMYB28* in overexpression lines and WT. (d) *RsMYB28*-OE transgenic plant. (e) The aliphatic glucosinolates (AGSLs) content in *RsMYB28*-OE lines and wild type (WT). (f) The indolic glucosinolates (IGSLs) content in *RsMYB28*-OE lines and WT. (g) The total glucosinolates (TGSLs) content in *RsMYB28*-OE lines and WT. Each value is the mean of three replicates. The vertical bar indicates the standard error. Asterisks indicate significant differences (** $p < 0.01$, * $p < 0.05$).

taste following extraction of oil for human consumption[43], only maintained the higher synthesis amount in R2260 leaves, and lower in seeds (Fig. 1a, d). Tailored to market demand, the identification of the GSLs profile provides the possibility for breeding cultivars with traits of special GSL accumulation. For rapeseed breeding, a scope was proposed, which was to reduce the antinutritional GSL and retaining, or increasing, the accumulation of other GSLs, to provide both unique flavors for the human diet and specific resistance to crop pests and pathogens.

The composition, accumulation, and distribution of GSLs vary among different species and genotypes, and the spatiotemporal distribution of GSLs in plants is modulated by developmental and

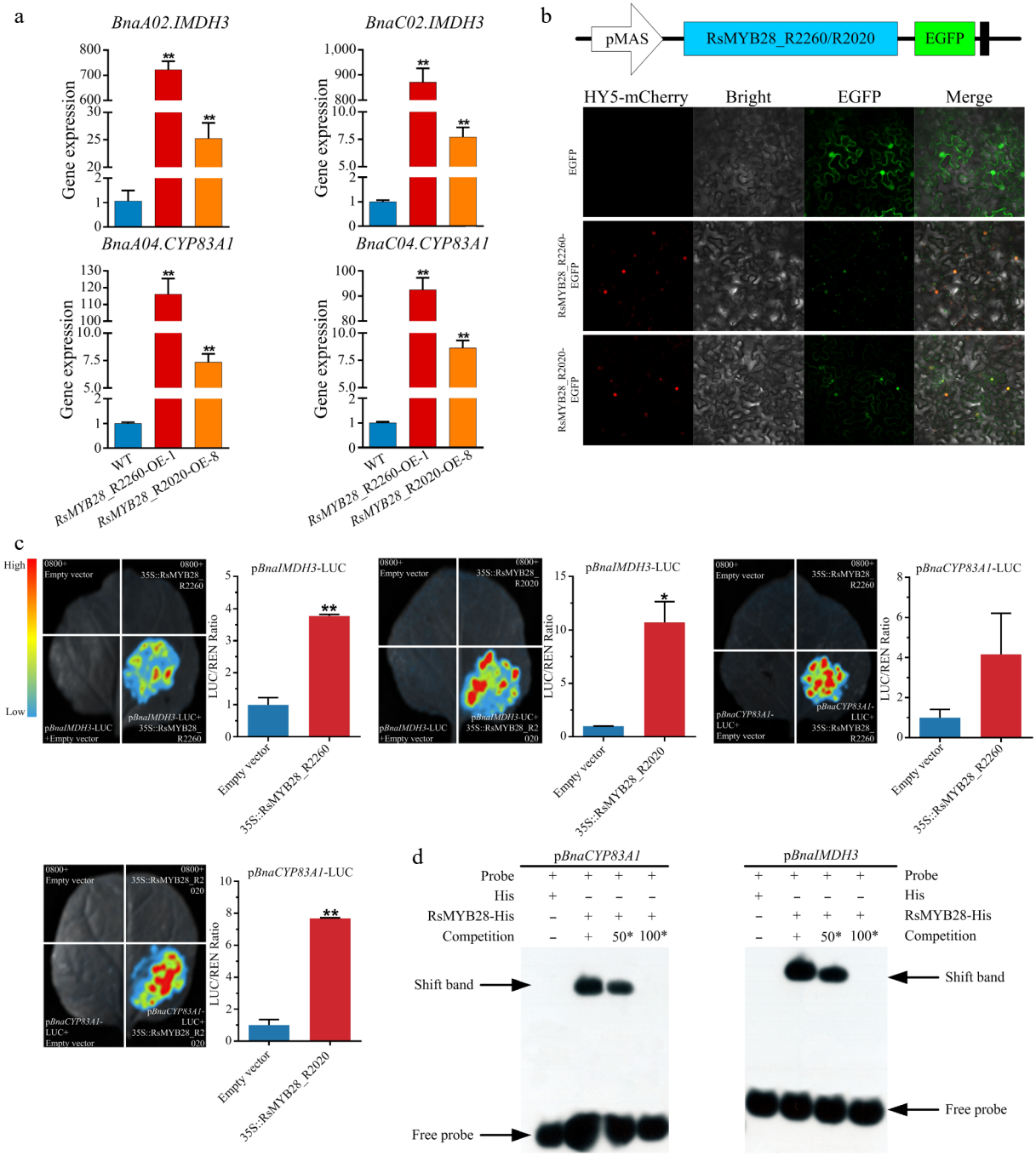

Fig. 6 RsMYB28 directly interact with the promoters of *BnaIMDH3* and *BnaCYP83A1*. (a) Relative expression of *BnaIMDH3* and *BnaCYP83A1* in RsMYB28-overexpressing (RsMYB28-OE) lines and wild type (WT). (b) Subcellular localization of RsMYB28 transcription factors. (c) Dual-luciferase reporter gene assay of RsMYB28 and promoters of *BnaIMDH3* and *BnaCYP83A1*. (d) Electrophoretic mobility shift assay of RsMYB28, and promoters of *BnaIMDH3* and *BnaCYP83A1*. Each value is the mean of three replicates. The vertical bar indicates the standard error. Asterisks indicate significant differences (** $p < 0.01$, * $p < 0.05$).

environmental regulations[34]. The main biosynthesis tissues of GSLs are young leaves, stems, roots, and developing silique walls, and during the reproductive phase, GSLs are transported to seeds from leaves, roots, and silique pericarps[44]. According to the present datasets, even though the GSLs were highly accumulated in the seeds of R2260, the gene expression remained at an extremely low level, GSL biosynthesis was activated in both silique pericarps and leaves (Figs. 2, 3), which indicated that a source-sink relationship is maintained between leaves/silique pericarps and seeds to facilitate GSL synthesis and accumulation. The investigation of GSLs long- and short-distance distributions from source to sink tissues in plants, three GSL transporters (GTR1, GTR2, and GTR3), and three GSL uniport exporters (UMAMIT29, UMAMIT30, and UMAMIT31) were identified[45,46]. Therefore, it is worth further developing a novel rapeseed germplasm with low seed-GSLS and high vegetative tissue GSLs.

The Brassica MYB28 orthologues share a high level of sequence conservation with MYB28 and have a close evolutionary relationship[47]. After genome polyploidization, the functional divergence occurred in different Brassica *MYB28* copies[48]. Five loci genes of *MYB28* were identified in the ZS11 genome, *BnaC02.MYB28*, *BnaA02.MYB28*, *BnaA03.MYB28*, *BnaC07.MYB28*, and

BnaC09.MYB28[49,50]. *BnaA09.MYB28* was deleted from low-GSL accessions according to Harper et al.[51]. With the quantification of GSL levels in 521 accession of seeds, eight loci (*GSL-A1*, *GSL-A2*, *GSL-A7*, *GSL-A10-1*, *GSL-C2-1*, *GSLC4-2*, *GSL-C8,* and *GSL-C9-2*) were specifically associated with seed-GSL. *GSL-A3* became a major locus associated with leaf-GSL variation in the low seed-GSL panel, and a 1,356 bp insertion in *BnaA3.MYB28* resulted in lower GSL content in leaves[42], the paralogs *BnA3.MYB28* and *BnC7.MYB28* within the homeologous regions shared the highest similarities, resulting in equally similar amino acid sequences[52] (Supplementary Fig. S4). *BnaC2.MYB28* and *BnaA2.MYB28* are significantly associated with the seed-GSLs content[48–50]. Additionally, *BnaC2.MYB28* was validated to be the major QTL (*qGSL-C2*) for SGC and the *BnaA2.MYB28* displayed high similarity with *BnaC2.MYB28*, however, *BnaC2.MYB28* contains a CACTA-like transposon insertion in the third exon, which disrupts the coding sequence of *BnaC2.MYB28,* and results in a dysfunctional protein[19].

MYB28 has been recognized as the predominant regulator for the synthesis of AGSLs. The sequence of *BnaMYB28s* in R2260 analysis indicated that the functional divergence occurred as with ZS11 (Fig. 4a, c, d, Supplementary Fig. S4c and S4d). The chromosomal locations of the Ogu fertility restorer gene and linked genes were mapped on the radish genomes, and the increased accumulation of AGSLs in R2260 of the present study subject, which allowed us to hypothesize that the foreign RsMYB28 play a key role in promoting AGSLs biosynthesis (Fig. 4b, Supplementary Fig. S3a and S3b). The positive regulation relationship have been confirmed between AtMYB28 and the AGSLs biosynthesis pathway genes (*AtMAM1*, *AtMAM3*, *AtBCAT4*, *AtCYP79F1*, *AtCYP79F2*, *AtCYP83A1*, *AtSOT17*, *AtSOT18,* and *AtAOP2*), and BnaC2.MYB28 formed homodimers and specifically interacted with BnaMYC3 co-regulated to activates the expression of *BnaBCAT4*, *BnaBAT5*, *BnaIMDH1*, *BnaIPMI2*, *BnaCYP83-A1*, and *BnaSOT17*[15,16,19]. To reveal the mechanism by which foreign RsMYB28 regulates AGSLs biosynthetic pathway genes in R2260. Overexpressed *RsMYB28* in rapeseed resulted in AGSLs accumulation, and the AGSLs biosynthesis pathway gene expression enhancement (Figs. 5, 6a). Moreover, RsMYB28 possessed the capacity to directly activate the transcription of *BnaIMDH3* and *BnaCYP83A1*, which are responsible for AGSL side chain elongation, and core structure formation. With the knowledge that foreign RsMYB28 plays an essential role in modulating AGSLs biosynthesis in rapeseed restorer line, there is a potential to engineer special AGSLs accumulation brassica crops, to endow crops with special flavors and health-promoting functions, while enhancing their resistance to pests and pathogens.

Author contributions

The authors confirm their contributions to the paper as follows: writing-original draft, conceptualization, visualization: Mao S; writing-review and editing: Mao S, Zhang D; formal analysis, investigation: Deng Y; data curation, validation: Deng Y, Zhu S; supervision: Zhang D, Yan M; investigation, validation: Cui J, He C; methodology: Mao S, Zhang D, Qin L, Liu L; resources: Wang T, Li B, Li M; funding acquisition: Mao S, Yan M; project administration, resources: Yan M. All authors reviewed the results and approved the final version of the manuscript.

Data availability

The sequence data from RNA-Seq experiments reported in this study have been deposited in Figshare (figshare.com), with the DOI: 10.6084/m9.figshare.30403486.

Acknowledgments

This work was supported by the National Key Research and Development Program of China (2023YFD1201403), the Natural Science Foundation of Hunan Province (2025JJ60173), the Science and Technology Innovation Program of Hunan Province (2023RC1077), the Hunan Provincial Science and Technology Talent Promotion Project (2023TJ-Z09), the Hunan Agricultural Sci-Tech Innovation Funding Project (2024CX032), the Yuelushan Laboratory Talent Program (2024RC2071), the Yuelushan Laboratory Breeding Program (YLS-2025-ZY02016).

Conflict of interest

The authors declare that they have no conflict of interest.

Supplementary information accompanies this paper at (https://www.maxapress.com/article/doi/10.48130/seedbio-0025-0021)

Dates

Received 25 June 2025; Revised 15 September 2025; Accepted 16 September 2025; Published online 28 November 2025

References

1. Qin H, King GJ, Borpatragohain P, Zou J. 2023. Developing multifunctional crops by engineering Brassicaceae glucosinolate pathways. *Plant Communications* 4:100565
2. Miao H, Xia C, Yu S, Wang J, Zhao Y, et al. 2023. Enhancing health-promoting isothiocyanates in Chinese kale sprouts via manipulating *BoESP*. *Horticulture Research* 10:uhad029
3. Fenwick GR, Heaney RK, Mullin WJ, VanEtten CH. 1983. Glucosinolates and their breakdown products in food and food plants. *C R C Critical Reviews in Food Science and Nutrition* 18:123–201
4. Griffiths DW, Birch ANE, Hillman JR. 1998. Antinutritional compounds in the *Brasi* Analysis, biosynthesis, chemistry and dietary effects. *The Journal of Horticultural Science and Biotechnology* 73:1–18
5. Arouisse B, Thoen MPM, Kruijer W, Kunst JF, Jongsma MA, et al. 2024. Bivariate GWA mapping reveals associations between aliphatic glucosinolates and plant responses to thrips and heat stress. *The Plant Journal* 120:674–86
6. Augustine R, Bisht NC. 2017. Regulation of glucosinolate metabolism: from model plant *Arabidopsis thaliana* to *Brassica* crops. In *Glucosinolates*, eds. Mérillon JM, Ramawat KG. Cham: Springer International Publishing. pp. 163–99 doi: 10.1007/978-3-319-25462-3_3 163-199
7. Salehin M, Li B, Tang M, Katz E, Song L, et al. 2019. Auxin-sensitive Aux/IAA proteins mediate drought tolerance in Arabidopsis by regulating glucosinolate levels. *Nature Communications* 10:4021
8. Yin X, Yang D, Zhao Y, Yang X, Zhou Z, et al. 2023. Differences in pseudogene evolution contributed to the contrasting flavors of turnip and Chiifu, two *Brassica rapa* subspecies. *Plant Communications* 4:100427
9. Engel E, Baty C, le Corre D, Souchon I, Martin N. 2002. Flavor-active compounds potentially implicated in cooked cauliflower acceptance. *Journal of Agricultural and Food Chemistry* 50:6459–67
10. Kitainda V, Jez JM. 2021. Structural studies of aliphatic glucosinolate chain-elongation enzymes. *Antioxidants* 10:1500
11. Kumar R, Lee SG, Augustine R, Reichelt M, Vassão DG, et al. 2019. Molecular basis of the evolution of methylthioalkylmalate synthase and the diversity of methionine-derived glucosinolates. *The Plant Cell* 31:1633–47
12. Harun S, Abdullah-Zawawi MR, Goh HH, Mohamed-Hussein ZA. 2020. A comprehensive gene inventory for glucosinolate biosynthetic pathway in *Arabidopsis thaliana*. *Journal of Agricultural and Food Chemistry* 68:7281–97

13. Liu S, Bartnikas LM, Volko SM, Ausubel FM, Tang D. 2016. Mutation of the glucosinolate biosynthesis enzyme cytochrome P450 83A1 monooxygenase increases camalexin accumulation and powdery mildew resistance. *Frontiers in Plant Science* 7:227
14. Liu G, He H, Wang P, Zhao X, Ren F. 2023. Glucoraphanin accumulation via glucoraphanin synthesis promotion during broccoli germination. *Foods* 13:41
15. Sønderby IE, Geu-Flores F, Halkier BA. 2010. Biosynthesis of glucosinolates – gene discovery and beyond. *Trends in Plant Science* 15:283–90
16. Mitreiter S, Gigolashvili T. 2021. Regulation of glucosinolate biosynthesis. *Journal of Experimental Botany* 72:70–91
17. Stracke R, Werber M, Weisshaar B. 2001. The *R2R3-MYB* gene family in *Arabidopsis thaliana*. *Current Opinion in Plant Biology* 4:447–56
18. Burow M, Atwell S, Francisco M, Kerwin RE, Halkier BA, et al. 2015. The glucosinolate biosynthetic gene *AOP2* mediates feed-back regulation of jasmonic acid signaling in *Arabidopsis*. *Molecular Plant* 8:1201–12
19. Zhou X, Zhang H, Xie Z, Liu Y, Wang P, et al. 2023. Natural variation and artificial selection at the *BnaC2. MYB28* locus modulate *Brassica napus* seed glucosinolate. *Plant Physiology* 191:352–68
20. Zhang Y, Yang Z, He Y, Liu D, Liu Y, et al. 2024. Structural variation reshapes population gene expression and trait variation in 2,105 *Brassica napus* accessions. *Nature Genetics* 56:2538–50
21. Feng J, Primomo V, Li Z, Zhang Y, Jan CC, et al. 2009. Physical localization and genetic mapping of the fertility restoration gene *Rfo* in canola (*Brassica napus* L.). *Genome* 52:401–7
22. Wang T, Guo Y, Wu Z, Xia S, Hua S, et al. 2020. Genetic characterization of a new radish introgression line carrying the restorer gene for Ogura CMS in *Brassica napus*. *PLoS One* 15:e0236273
23. Huang W, Gao GY, Wu JF, Liu LL, Zhang DW, et al. 2022. Regulation of flavonoid synthesis by *BjA09.TT8* and *BjB08.TT8* genes in *Brassica juncea*. *Acta Agronomica Sinica* 48:1169–80
24. Mao S, Wang J, Wu Q, Liang M, Yuan Y, et al. 2020. Effect of selenium–sulfur interaction on the anabolism of sulforaphane in broccoli. *Phytochemistry* 179:112499
25. Lamesch P, Berardini TZ, Li D, Swarbreck D, Wilks C, et al. 2012. The Arabidopsis information resource (TAIR): improved gene annotation and new tools. *Nucleic Acids Research* 40:D1202–D1210
26. Liu Z, Li N, Yu T, Wang Z, Wang J, et al. 2022. The Brassicaceae genome resource (TBGR): a comprehensive genome platform for Brassicaceae plants. *Plant Physiology* 190:226–37
27. Zhang X, Liu T, Wang J, Wang P, Qiu Y, et al. 2021. Pan-genome of *Raphanus* highlights genetic variation and introgression among domesticated, wild, and weedy radishes. *Molecular Plant* 14:2032–55
28. Chen C, Wu Y, Li J, Wang X, Zeng Z, et al. 2023. TBtools-II: a "one for all, all for one" bioinformatics platform for biological big-data mining. *Molecular Plant* 16:1733–42
29. Zhang D, Gao F, Jakovli I, Zou H, Zhang J, et al. 2020. PhyloSuite: an integrated and scalable desktop platform for streamlined molecular sequence data management and evolutionary phylogenetics studies. *Molecular Ecology Resources* 20:348–55
30. Lescot M, Déhais P, Thijs G, Marchal K, Moreau Y, et al. 2002. PlantCARE, a database of plant cis-acting regulatory elements and a portal to tools for in silico analysis of promoter sequences. *Nucleic Acids Research* 30:325–27
31. Sønderby IE, Hansen BG, Bjarnholt N, Ticconi C, Halkier BA, et al. 2007. A systems biology approach identifies a R2R3 MYB gene subfamily with distinct and overlapping functions in regulation of aliphatic glucosinolates. *PLoS ONE* 2:e1322
32. Kittipol V, He Z, Wang L, Doheny-Adams T, Langer S, et al. 2019. Genetic architecture of glucosinolate variation in *Brassica napus*. *Journal of Plant Physiology* 240:152988
33. Bazzaz FA, Chiariello NR, Coley PD, Pitelka LF. 1987. Allocating resources to reproduction and defense. *BioScience* 37:58–67
34. Malhotra B, Kumar P, Bisht NC. 2023. Defense versus growth trade - offs: insights from glucosinolates and their catabolites. *Plant, Cell & Environment* 46:2964–84
35. Cardozo LFMF, Alvarenga LA, Ribeiro M, Dai L, Shiels PG, et al. 2021. Cruciferous vegetables: rationale for exploring potential salutary effects of sulforaphane-rich foods in patients with chronic kidney disease. *Nutrition Reviews* 79:1204–24
36. Wu Q, Mao S, Huang H, Liu J, Chen X, et al. 2024. Chromosome-scale reference genome of broccoli (*Brassica oleracea* var. *italica* Plenck) provides insights into glucosinolate biosynthesis. *Horticulture Research* 11:uhae063
37. Mao S, Wang J, Guo Z, Huang H, Wang S, et al. 2025. Improving sulforaphane content in broccoli sprouts by applying Se: transcriptome profiling and coexpression network analysis provide insights into the mechanistic response. *Physiologia Plantarum* 177:e70037
38. Mocniak LE, Elkin KR, Dillard SL, Bryant RB, Soder KJ. 2023. Building comprehensive glucosinolate profiles for brassica varieties. *Talanta* 251:123814
39. Kaiser AE, Baniasadi M, Giansiracusa D, Giansiracusa M, Garcia M, et al. 2021. Sulforaphane: a broccoli bioactive phytocompound with cancer preventive potential. *Cancers* 13:4796
40. Ordonez AA, Bullen CK, Villabona-Rueda AF, Thompson EA, Turner ML, et al. 2022. Sulforaphane exhibits antiviral activity against pandemic SARS-CoV-2 and seasonal HCoV-OC43 coronaviruses in vitro and in mice. *Communications Biology* 5:242
41. Uddin MS, Al Mamun A, Jakaria M, Thangapandiyan S, Ahmad J, et al. 2020. Emerging promise of sulforaphane-mediated Nrf2 signaling cascade against neurological disorders. *Science of The Total Environment* 707:135624
42. Liu S, Huang H, Yi X, Zhang Y, Yang Q, et al. 2020. Dissection of genetic architecture for glucosinolate accumulations in leaves and seeds of *Brassica napus* by genome-wide association study. *Plant Biotechnology Journal* 18:1472–84
43. Bell L, Oloyede OO, Lignou S, Wagstaff C, Methven L. 2018. Taste and flavor perceptions of glucosinolates, isothiocyanates, and related compounds. *Molecular Nutrition & Food Research* 62:1700990
44. Jørgensen ME, Nour-Eldin HH, Halkier BA. 2015. Transport of defense compounds from source to sink: lessons learned from glucosinolates. *Trends in Plant Science* 20:508–14
45. Xu D, Sanden NCH, Hansen LL, Belew ZM, Madsen SR, et al. 2023. Export of defensive glucosinolates is key for their accumulation in seeds. *Nature* 617:132–38
46. He Y, Yang Z, Tang M, Yang QY, Zhang Y, et al. 2022. Enhancing canola breeding by editing a glucosinolate transporter gene lacking natural variation. *Plant Physiology* 188:1848–51
47. Hirai MY, Sugiyama K, Sawada Y, Tohge T, Obayashi T, et al. 2007. Omics-based identification of *Arabidopsis* Myb transcription factors regulating aliphatic glucosinolate biosynthesis. *Proceedings of the National Academy of Sciences of the United States of America* 104:6478–83
48. Liu Y, Zhou X, Yan M, Wang P, Wang H, et al. 2020. Fine mapping and candidate gene analysis of a seed glucosinolate content QTL, *qGSL-C2*, in rapeseed (*Brassica napus* L.). *Theoretical and Applied Genetics* 133:479–90
49. Sun F, Fan G, Hu Q, Zhou Y, Guan M, et al. 2017. The high - quality genome of *Brassica napus* cultivar 'ZS11' reveals the introgression history in semi-winter morphotype. *The Plant Journal* 92:452–68
50. Lu G, Harper AL, Trick M, Morgan C, Fraser F, et al. 2014. Associative transcriptomics study dissects the genetic architecture of seed glucosinolate content in *Brassica napus*. *DNA Research* 21:613–25
51. Harper AL, Trick M, Higgins J, Fraser F, Clissold L, et al. 2012. Associative transcriptomics of traits in the polyploid crop species *Brassica napus*. *Nature Biotechnology* 30:798–802
52. Long Y, Wang J, Wang Y, Zhang J, Wang J, et al. 2016. Comparative analysis of *MYB28* homologs and development of a *MYB28*-specific marker in *Brassica napus* L. *Molecular Breeding* 36:126